IEEE Access
Multidisciplinary | Rapid Review | Open Access Journal

Received December 6, 2020, accepted December 11, 2020, date of publication December 17, 2020,
date of current version December 31, 2020.

Digital Object Identifier 10.1109/ACCESS.2020.3045598

Positioning Accuracy Improvement of Industrial Robots Considering Configuration and Payload Effects via a Hybrid Calibration Approach

JEN-CHUNG HSIAO[1], KUMAR SHIVAM[1], I-FANG LU[1], AND TAI-YAN KAM[2]
[1]Precision Machinery Research & Development Center (PMC), Taichung City 40768, Taiwan, R.O.C.
[2]Department of Mechanical Engineering, National Chiao Tung University, Hsinchu 30010, Taiwan, R.O.C.

Corresponding author: Jen-Chung Hsiao (e8222@mail.pmc.org.tw)

This work was supported in part by the Technology Development Program of DoIT of Taiwan (R.O.C.) under Grant 109-EC-17-A-25-1517.

ABSTRACT Robot calibration of an industrial robot is of importance for those applications requiring high positioning accuracy. The use of numerical optimization techniques to identify the accurate kinematic parameters and tackle the residual errors for improving positioning accuracy is still challenging. The difficulties in using the conventional optimization techniques is associated with the expensive computation of the second derivative terms in the Hessian matrix and even more linked to the additional improvement of the residual errors induced by the configuration and payload effects for the practical applications. A hybrid calibration procedure, which is robust and efficient, is proposed to handle the said problems in this study. The first step is to utilize the Broyden–Fletcher–Goldfarb–Shanno (BFGS) algorithm together with the quasi-Newton method to optimize the cost function with non-smooth nature established using massive measurement data. In the second step, two kinds of artificial neural network (ANN) algorithms are employed to further improve the nonlinear residual errors induced by payload and configuration effects. After the completion of the hybrid calibration, improvements of 88.1% and 80.1% have been attained, respectively, for the mean and maximum positioning errors of the robot end-effector, i.e., the mean/maximum positioning errors are reduced from 2.613mm/6.294mm to 0.310mm/1.255mm for 840 untrained measurement data. The experimental results also validated the effectiveness of the proposed method.

INDEX TERMS Artificial neural network, BFGS algorithm, industrial robots, robot calibration.

I. INTRODUCTION

Nowadays, facing the megatrend for smart factories of the future, an industrial robot plays an increasingly important role in not only traditional pick-and-place tasks but also many new applications such as assembling, welding, measuring, and machining. These robots must have high accuracy and efficiency to satisfy the requirements of precision operations. In general, the industrial robots presently available have better performance in repeatability than in positioning accuracy. Regarding positioning accuracy improvement, the utilization of teaching pendant to mitigate the poor positioning accuracy is a very common practice. Such practice, however, may not be viable for the applications that need precision processes or necessitate the use of off-line programming for large and complex workpieces. Furthermore, the practice is also a time-consuming and inefficient process besides its dissatisfaction of path tracking accuracy. Therefore, the task of improving the positioning accuracy of industrial robots has become an active and interesting topic of research.

The positioning accuracy of industrial robots is affected by multiple factors such as kinematic parameter errors, joint flexible deformation, and link deformation. The positioning accuracy of the conventional robots usually lies in the range of one to several millimeters, which cannot achieve the high precision requirements. To develop an industrial robot with higher positioning accuracy, several ways have been proposed to enhance its performance through the applications of design optimization, optimal control algorithm, and robot calibration. Although the positioning accuracy of an industrial robot has been improved via the design and control approaches in the past two decades, it is still hard to reach the goal of attaining the required accuracy due to the following reasons: 1) the geometric effects such as small shape/size deviations of the joints and links of robot will cause substantial errors

The associate editor coordinating the review of this manuscript and approving it for publication was Pedro Neto.

at the end-effector. 2) the contradiction between the lighter weight and higher rigidity of a link makes the link design a compromised result evolved from the trade-off between the link weight and rigidity. 3) the geometric deviations of joints and links when coupled with their weight effects may cause additional positioning errors at different robot configurations. However, after the design and control optimizations have been implemented, robot calibration can play a significantly vital role to improve the positioning accuracy of industrial robots.

Without rearranging or redesigning the robot, robot calibration can be used to improve the positioning accuracy of an industrial robot in a sequential process which involves the steps of modeling, measurement, identification, and compensation. Roth *et al.* [1] divided the domain of robot calibration into three levels, i.e., level-1, level-2, and level-3. Level-1 calibration is to identify the correct relationships between the signal produced by the joint displacement sensor and the actual joint displacement. Level-2 calibration is to aim at the determination of the kinematic geometries of the robot as well as the joint-angle relationship. Level-2 is also termed as ''kinematic'' or ''geometric'' calibration, which covers assembly errors, machining errors, and joint angles offset, i.e., the deviations of nominal kinematic parameters from the actual parameters. Level-3 calibration is defined as ''non-kinematic'' or ''non-geometric'' calibration, which may account for the effects of servo error, backlash and friction of gearbox, link elastic and thermal deformations, link compliance, and payload. It is noted that the research issues in level-1 and level-2 calibrations have drawn close attention in the past two decades [2]–[5]. To further enhance the robot accuracy, some researchers [6]–[11] have attempted to tackle the issues of the complex level-3 calibration, which involve the parameter identification with geometric and non-geometric errors of industrial robots, to meet the demand for higher precision. For example, Jang *et al.* [6] and Zhou *et al.* [9] proposed a similar method to consider not just the kinematic model but also joint stiffness model using linear torsional spring to compensate the positioning errors. Meggiolaro *et al.* [12] explicitly decomposed measured end-point error data into generalized geometric and elastic deformation errors. Their method, being simple in computation, only requires determining the parameters of which each is dependent of one variable. The works done in the area of robot calibration have led to some improvements of the positioning accuracy of industrial robots in recent years.

There are many non-geometric error sources, which cannot be modeled correctly and completely. For instance, in the above-mentioned joint stiffness model, only the effects of joint deflection are taken into account. Hence, some researchers [13]–[15] have studied other solutions to model the overall non-geometric errors using an artificial neural network (ANN) technique to reduce the robot positioning error. For instance, Jang *et al.* [6] proposed a radial basis function network (RBFN) to describe the relationship between robot joint offset errors with end-effector positions. Wang *et al.* [16] also utilized an ANN to describe the functional relationship between end-effector positions and their corresponding positioning errors. Takanashi [17] applied a multiple layer ANN to approximate the relationship between robot joint positions and the associated joint offset errors. These works have given a new research direction for modeling the non-geometric errors of an industrial robot. However, in the previous works, there remain some problems to be further solved: 1) the geometric parameter identification techniques for cost functions with non-smooth nature under massive measurements should be studied in-depth to increase the computational robustness and efficiency. 2) only a few studies have discussed the loading effects, mostly focused on the static weight of link and end-effector only. Payload effects, which were not considered in most of the previous works, should be considered in real engineering cases. 3) the positioning accuracy is closely related to the factors of loading condition and robot configuration. Most of the previous works did not consider these two factors simultaneously for robot calibration.

In this paper, the enhancement of the positioning accuracy on the PMC6VA030 industrial robot using the quasi-Newton optimization and ANN techniques is achieved via a hybrid robot calibration approach. First, based on the kinematic model of an industrial robot, the geometric parameters, definition of positioning error, and objective functions of the optimization problem are defined. Next, a quadratic error model is chosen for optimizing the kinematic parameters under extensive measurements without loading effect at 168 different configurations. In solving the optimization problem, the Broyden–Fletcher–Goldfarb–Shanno (BFGS) algorithm, which is robust and efficient, is employed to minimize the cost function with non-smooth nature. Two artificial neural network methods with different outputs and models are used to further improve the residual positioning error without constraints on configuration and loading. The proposed paper is able to make two significant contributions: One is to provide a robust calibration approach for robot positioning accuracy improvement using the BFGS optimization and ANN techniques to attain high position accuracy in an efficient way; the other is to solve the robot calibration problem of an industrial robot considering non-geometric errors, payload, and robot configuration effects simultaneously for achieving high position accuracy.

The rest of the paper is organized as follows. Section II introduces the system kinematics, error model, and problem formulation. Section III elaborates the BFGS and ANN-based methods used in the proposed hybrid calibration approach. Section IV describes the experimental setup for positioning measurement of the PMC6VA030 six-axis industrial robot. Section V is to show the experimental results and compare the error results predicted using different methods. Section VI is the conclusions and future works.

II. SYSTEM MODEL AND PROBLEM FORMULATION

A. SYSTEM DESCRIPTION

1) THE EXPERIMENTAL TESTBED

The PMC6VA030 robot, a six-axis industrial robot shown in Fig. 1, is fabricated by PMC, Taiwan. The maximum payload and reach are 30 kgf and 1800 mm, respectively. The structure of the robot is composed of six revolute joints and six robot arms. Each robot arm is driven by a joint module which consists of servo motor, reduction gear, and encoder.

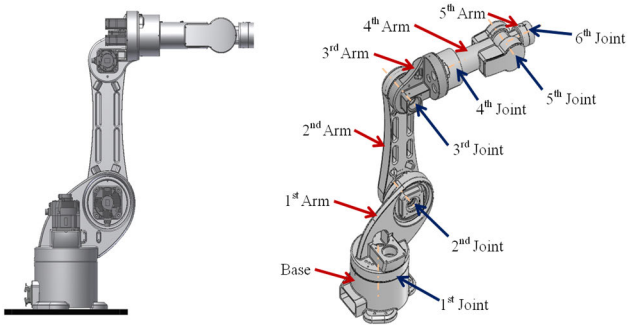

FIGURE 1. The architecture of PMC6VA030 industrial robot.

2) THE KINEMATIC AND ERROR MODELS

The kinematic model of PMC6VA030 robot is based on the modified Denavit and Hartenberg (MDH) notation [18], four kinematic parameters (joint angle θ_i, offset distance d_i, link length a_i and twist angle α_i) are used to describe the translation and rotation between two adjacent links. The transformation from link frame $\{i-1\}$ to link frame $\{i\}$ can be expressed by a homogeneous matrix $\boldsymbol{A}_i^{i-1}$. The matrix is described as

$$\begin{aligned}\boldsymbol{A}_i^{i-1} = &\boldsymbol{Rot}\,(x_{i-1},\alpha_{i-1})\,\boldsymbol{Trans}\,(x_{i-1},a_{i-1})\ldots\\ &\boldsymbol{Rot}\,(z_i,\theta_i)\,\boldsymbol{Trans}\,(z_i,d_i)\end{aligned}\tag{1}$$

To solve the problem of two consecutive joints in parallel or near parallel (See 2nd joint and 3rd joint in Fig. 1), a small rotation β_1 about the y-axis must be taken into account [19].

The kinematic scheme of the PMC6VA030 robot is shown in Fig. 2 and its nominal kinematic parameters are listed in Table 1.

TABLE 1. Nominal kinematic parameters of PMC6VA030 robot.

Joint i	a_{i-1}	α_{i-1}	β_{i-1}	d_i	θ_i
1	0	180	-	-601	0
2	270	90	0	0	0
3	800	0	-	0	0
4	140	90	-	-737.5	0
5	0	-90	-	0	0
6	0	-90	-	227.3	0

In the experimental system, a laser tracker is used to collect the position data and the laser sensor base frame $\{s\}$ is considered as the fixed (world) frame. The laser tracker and retro-reflector are located near the robot base and attached to

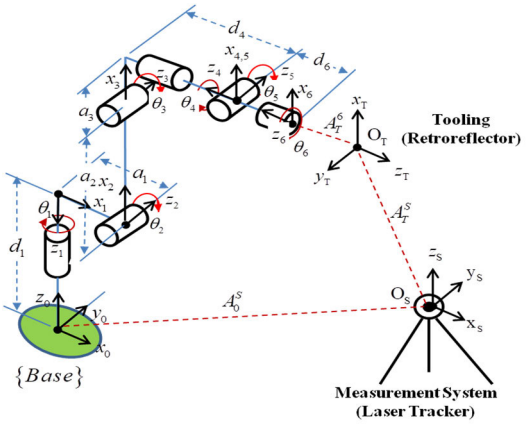

FIGURE 2. The kinematic scheme of a robot-laser tracker system.

the robot end-fffector, respectively. The robot base frame $\{o\}$ is defined by six parameters with respect to the laser sensor frame $\{s\}$ as shown in Fig. 2. The position and orientation of the retro-reflector with respect to the sensor-base frame $\{s\}$ can be expressed as the following successive multiplications of the transformation matrices.

$$\boldsymbol{A}_T^s = \boldsymbol{A}_1^s\boldsymbol{A}_2^1\boldsymbol{A}_3^2\boldsymbol{A}_4^3\boldsymbol{A}_5^4\boldsymbol{A}_6^5\boldsymbol{A}_T^6 = \begin{bmatrix}\boldsymbol{R}_T^s & \boldsymbol{P}_T^s\\ 0 & 1\end{bmatrix}\tag{2}$$

where $\boldsymbol{R}_T^s$ and $\boldsymbol{P}_T^s$ represent the orientation matrix and position vector of the retro-reflector with respect to the sensor-base frame $\{s\}$, respectively. No loss in generality, hereafter, just $\boldsymbol{P}_T^s$ is considered as the target of this study.

Herein, the accuracy correction of industrial robots is mainly to minimize the error between the actual position and the nominal position of the robot end-effector point to achieve accuracy improvement. Taylor series will be expanded at the position calculated by the nominal kinematic parameters, which can be approximated as

$$\boldsymbol{P}_r \approx \boldsymbol{P}_n + \Delta\boldsymbol{P}_{err} = f\left(\boldsymbol{q}_n\right) + \left(\partial f\,/\,\partial\boldsymbol{q}\right)\Delta\boldsymbol{q}\tag{3}$$

where $\boldsymbol{P}_r$ is the real position of end-effector point, $\boldsymbol{P}_n$ is the nominal position of end-effector point computed based on the nominal kinematic parameters of the industrial robot, $\Delta\boldsymbol{P}_{err}$ is the positioning error between $\boldsymbol{P}_r$ and $\boldsymbol{P}_n$, $\boldsymbol{q} = [a\ \alpha\ \beta\ d\ \theta]^T$ is a generalized vector of kinematic parameters.

The positioning error model is expressed as

$$\Delta\boldsymbol{P}_{err} = \left(\partial f\,/\,\partial\boldsymbol{q}\right)\Delta\boldsymbol{q} = J_{\boldsymbol{q}}\Delta\boldsymbol{q}\tag{4}$$

where and $J_{\boldsymbol{q}} = [J_\alpha J_\alpha J_\beta J_d J_\theta]$ is a $3\times n$ extended kinematic Jacobian matrix. $\Delta\boldsymbol{q} = [\Delta\alpha\Delta a\Delta\beta\Delta d\,\Delta\theta]^T$ is a $n\times 1$ kinematic parameter error vector, n is the number of kinematic parameters which will be calibrated. Its least square solution is

$$\Delta\boldsymbol{q} = \left(J_{\boldsymbol{q}}^T J_{\boldsymbol{q}}\right)^{-1} J^T\Delta\boldsymbol{P}_{err}\tag{5}$$

Equation (15) is the called steepest-descent method with the first-order derivative information. However, if the second-order derivative is available, it can be used to represent the

cost surface accurately, and a better search direction and rate of convergence can be found. The second-order Taylor's expansion can be written as [20]

$$\boldsymbol{P}_r \approx f\left(\boldsymbol{q}_n\right) + \nabla f^T \boldsymbol{c} + \frac{1}{2}\boldsymbol{c}^T \boldsymbol{H}\boldsymbol{c} \tag{6}$$

where $\mathbf{c} = \nabla f$ denotes the gradient vector, and $\boldsymbol{H}$ is the Hessian matrix. The search direction can be obtained

$$\Delta \boldsymbol{q} = -\boldsymbol{H}^{-1}\boldsymbol{c} \tag{7}$$

Once Δq is available, the design is updated as

$$\boldsymbol{q}^{(i)} = \boldsymbol{q}^{(i-1)} + \Delta \boldsymbol{q} \tag{8}$$

3) MODELING RESIDUAL ERRORS OF A ROBOT WITH PAYLOAD

The real position vector $\boldsymbol{P}_r$ of the robot end-effector can be expressed as

$$\boldsymbol{P}_r = \boldsymbol{P}_{kin} + \Delta \boldsymbol{P}_{err} \tag{9}$$

where $\boldsymbol{P}_{kin}$ is the command position based on nominal kinematic parameters built in the robot controller, and $\Delta \mathrm{P}_{\mathrm{err}}$ represents the positioning error which is the difference between the real position and command position. Here, $\Delta \mathrm{P}_{\mathrm{err}}$ can be divided into two main parts.

$$\Delta \boldsymbol{P}_{err} = \boldsymbol{P}_r - \boldsymbol{P}_{kin} = \Delta \boldsymbol{P}_{kin} + \Delta \boldsymbol{P}_{resil} \tag{10}$$

$$\Delta \boldsymbol{P}_{resil} = \Delta \boldsymbol{P}_{joint} + \Delta \boldsymbol{P}_{link} + \Delta \boldsymbol{P}_{others} \tag{11}$$

In (20), $\Delta \boldsymbol{P}_{kin}$ is the positioning error caused by kinematic error, and $\Delta \boldsymbol{P}_{resil}$ represents the residual positioning error caused by non-geometric factors except kinematic error. In (21), the residual error is further divided into $\Delta \boldsymbol{P}_{joint}$, $\Delta \boldsymbol{P}_{link}$, and $\Delta \boldsymbol{P}_{others}$, which denote, respectively, the errors caused by joint deflection, link deformation, and other non-geometric error such as backlash, friction, and thermal deformation. It is difficult to model them using an analytical formulation because of the nonlinearity and complexity. Moreover, $\Delta \boldsymbol{P}_{joint}$ and $\Delta \boldsymbol{P}_{link}$ are not only related to robot configurations, but also significantly affected by the payload at the robot end-effector in real engineering applications. In view of the above issues, the residual positioning error of the robot under loads at different configurations can be expressed as

$$\Delta \boldsymbol{P}_{resil,j} = f\left(\boldsymbol{\theta}_i, \boldsymbol{L}_m\right) \tag{12}$$

where $\boldsymbol{\theta}_i$ is the i$^{\mathrm{th}}$ robot joint angle and $\boldsymbol{L}_m$ denotes the m$^{\mathrm{th}}$ loading condition.

B. PROBLEM FORMULATION

The goal of robot calibration is to identify the parameters of kinematic and non-kinematic models so that the difference between theoretical and measured end-effector positions can be minimized. Given an industrial robot with n joints and kinematic model $\boldsymbol{f}$, the computed position $\boldsymbol{P}_{kin}$ of end-effector is given by:

$$\boldsymbol{P}_{kin} = f\left(\boldsymbol{q}\right), \quad \boldsymbol{P} \in SEG \tag{13}$$

where $\boldsymbol{q} \in R^{i\times 1}$ is the kinematic parameters with i being the number of joints of the robot; SEG stands for the Special Euclidean Group.

Here, the problem of robot calibration can be viewed as an optimization problem such that the difference between computed position $\boldsymbol{P}_c$ and measured position $\boldsymbol{P}_m$ is minimized.

$$min \left\|\boldsymbol{P}_m - \boldsymbol{P}_c\right\| = min \left\|\Delta \boldsymbol{P}_{err}\right\| \tag{14}$$

The first step is to minimize the kinematic error, which is formulated as, shown at the bottom of this page.

where n is the number of samples, RMS is an acronym of root mean square.

The second step is to minimize the residual error, which is expressed as

$$min\ RMS\left(\Delta \boldsymbol{P}_{resil}\right) = min\ RMS\left(\Delta \boldsymbol{P}_{err} - \Delta \boldsymbol{P}_{kin}\right) \tag{16}$$

III. TECHNIQUES FOR THE PROPOSED HYBRID ROBOT CALIBRATION APPROACH

The flowchart of the proposed hybrid calibration approach which adopts two-step optimization processes to address, respectively, the kinematic error using BFGS and the residual positioning error using two kinds of ANN-based compensation for minimizing the positioning error is shown in Fig. 3. In this section, two core techniques, namely, BFGS algorithm, single-output multi-model ANN (hereafter termed as SOMM-ANN) technique, and classified aided SOMM-ANN (hereafter termed as CA-SOMM-ANN) technique of the proposed hybrid calibration approach will be introduced.

It is noted that in the optimization theory, the second-order Newton method usually has higher accuracy and convergence than the first-order Newton method, i.e., the gradient method. But the use of the second-order Newton method is required to calculate the second-order Hessian and its inverse matrix, which may be computationally expensive and tedious. The BFGS algorithm adopted herein is a quasi-Newton method which uses an approximation (first order derivative) to compute either the Jacobian or the Hessian matrix for obtaining the efficiency and convergence. Although the use of BFGS may induce some small accuracy loss, this accuracy loss can be compensated when performing the ANN-based process in the proposed hybrid calibration.

$$min\ RMS\left(\Delta \boldsymbol{P}_{err}\right) = min\left(\frac{1}{n-1}\sum\nolimits_{i=1}^{n}\sqrt{\left(\left(\Delta \boldsymbol{P}_{errx}\right)^2 + \left(\Delta \boldsymbol{P}_{erry}\right)^2 + \left(\Delta \boldsymbol{P}_{errz}\right)^2\right)}\right) \tag{15}$$

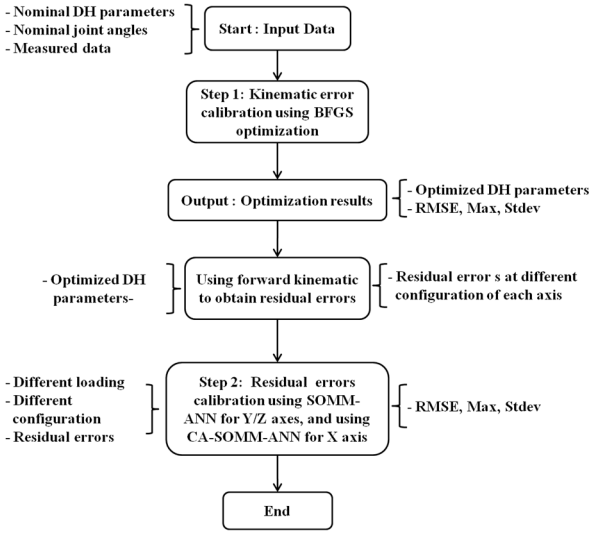

FIGURE 3. The flowchart of the proposed hybrid calibration approach.

The positioning error can be decomposed to three axial error components in, respectively, the X, Y, and Z directions. It is noted that the use of the traditional ANN using a single model to train the input and output relationship may encounter difficulty for predicting optimal parameters. Herein, the multi-model SOMM-ANN and CA-SOMM-ANN techniques established on the basis of the axial error components are used to perform the training process for predicting optimal parameters.

A. BFGS ALGORITHM FOR IDENTIFICATION OF KINEMATIC PARAMETERS

The BFGS algorithm is an iterative procedure to seek a stationary point of the cost function (preferably to be twice continuously differentiable). It can have acceptable performance even for non-smooth optimization problems. The steps for the stationary point search are summarized in the following [20]:

Step 1: Estimate an initial design point for DH parameters, $\boldsymbol{x}^{(0)}$. Choose a symmetric, positive, and definite $n \times n$ matrix, $\boldsymbol{H}^{(0)}$ as an estimate for the Hessian of the cost function (mean squared error). In the absence of more information, let $\boldsymbol{H}^{(0)} = \boldsymbol{I}$. Choose a convergence tolerance parameter, ε. Then set $k = 0$ and compute the gradient vector as $\boldsymbol{c}^{(0)} = \nabla f(\boldsymbol{x}^{(0)})$. The cost function, $\boldsymbol{f}(x)$ is defined as the error between the forward kinematic position values of DH parameters at different fixed angle configurations, Θ and the measured positioning errors in (15).

$$f\left(\boldsymbol{x}^{(k)}\right) = RMS\left(\Delta \boldsymbol{P}_{kin}\right), \quad for\ \boldsymbol{A}_T^s(\boldsymbol{x}^{(k)}, \Theta) \tag{17}$$

Step 2: Calculate the norm of the gradient vector as $||\boldsymbol{c}^{(k)}||$. If $||\boldsymbol{c}^{(k)}|| < \varepsilon$, stop the iterative process; otherwise, continue.

Step 3: Solve the following linear system of equations to obtain the search direction:

$$\boldsymbol{H}^{(k)}\boldsymbol{d}^{(k)} = -\boldsymbol{c}^{(k)} \tag{18}$$

Step 4: Compute the optimum step size:

$$\alpha_k = \alpha\ to\ minimize\ f\left(\boldsymbol{x}^{(k)} + \alpha \boldsymbol{d}^{(k)}\right) \tag{19}$$

Step 5: Update the design as

$$\boldsymbol{x}^{(k+1)} = \boldsymbol{x}^{(k)} + \alpha_k \boldsymbol{d}^{(k)} \tag{20}$$

Step 6: Update the Hessian approximation for the cost function as

$$\boldsymbol{H}^{(k+1)} = \boldsymbol{H}^{(k)} + \boldsymbol{D}^{(k)} + \boldsymbol{E}^{(k)} \tag{21}$$

where the correction matrices $\boldsymbol{D}^{(k)}$ and $\boldsymbol{E}^{(k)}$ are given as

$$\boldsymbol{D}^{(k)} = \boldsymbol{y}^{(k)}\boldsymbol{y}^{(k)T} \Big/ \left(\boldsymbol{y}^{(k)} \cdot \boldsymbol{s}^{(k)}\right) \tag{22}$$

$$\boldsymbol{E}^{(k)} = \boldsymbol{c}^{(k)}\boldsymbol{c}^{(k)T} \Big/ \left(\boldsymbol{c}^{(k)} \cdot \boldsymbol{d}^{(k)}\right) \tag{23}$$

where

$$\boldsymbol{s}^{(k)} = \alpha_k \boldsymbol{d}^{(k)}(change\ in\ design) \tag{24}$$

$$\boldsymbol{y}^{(k)} = \boldsymbol{c}^{(k+1)} - \boldsymbol{c}^{(k)}(change\ in\ gradient) \tag{25}$$

$$\boldsymbol{c}^{(k+1)} = \nabla f(\boldsymbol{x}^{(k+1)}) \tag{26}$$

Step 7: Set $k = k + 1$ and go to Step 2.

B. SINGLE-OUTPUT MULTI-MODEL ANN (SOMM-ANN) FOR COMPENSATING THE RESIDUAL ERROR

As well known, it is difficult to model the non-geometric error sources such as link stiffness, gear backlash, and others correctly and completely. To tackle this difficulty, an artificial neural network has been proposed to compensate the robot positioning errors in the previous studies [16], [17]. The model-based optimization method using DH-parameters can reduce the overall positioning error of industrial robots down to a reasonable value. For some precision applications, however, the achieved positioning errors of the robot are still considered to be relatively large. The DH-parameters based kinematic model only takes the geometric errors into account and fails to capture the loading effect as well as other nonlinear errors. Some studies [13]–[15] utilized ANN-based method to reduce the overall positioning error by taking both geometric and non-geometric errors into account. Herein, the individual axis error of the positioning error with the considering of non-geometric effects will be predicted using the aforementioned SOMM-ANN technique. The architecture of the SOMM-ANN model used for modeling load effect is shown in Fig. 4. By comparing with the previous work [13], the proposed SOMM-ANN model can provide better generalization of the error for the trained axis because the model only learns the error of one axis as a function of payload and joint angles.

In the training of the SOMM-ANN model, the control angles $\theta_d\,[\theta_1, \theta_2, \theta_3, \theta_4, \theta_5, \theta_6]$ and the effective loading L_d [w] at the end-effector are treated as the input data. The output variables are considered as the positioning errors $p_e\,[x_e, y_e, z_e]$ for each axis. The SOMM-ANN models of X, Y and Z axes consist of 6, 2 and 4 hidden layers, respectively. The hyper-parameters and training parameters of the

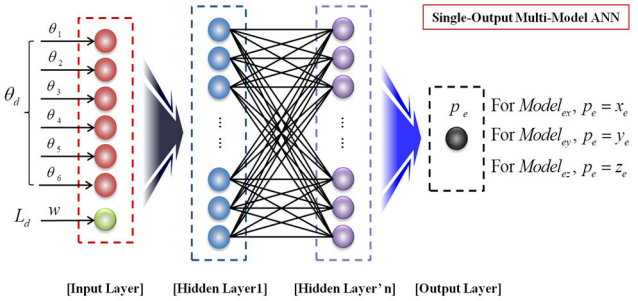

FIGURE 4. SOMM-ANN architecture used to model non-geometric positioning errors with loading and configuration effects.

TABLE 2. Hyper-parameters of SOMM-ANN model.

Layer Name	X axis model	Y axis model	Z axis model
Optimizer	Adam	Adam	Adam
Learning rate	0.0008	0.0005	0.001
Epoch	200	200	200
Batch size	200	200	200

proposed models are listed in TABLE 2 and TABLE 3, respectively. The numbers of hidden layers, neurons in each layer and the activation functions are obtained via the 'Tree of Parzen Estimators' [21] approach provided in the Hyperopt/Python library [22].

We use mean squared error as our loss function to train the above SOMM-ANN model and the first-order gradient-based optimizer Adam [23] to optimize the model. An early stopping method is adopted to stop training if the training loss doesn't improve for 5 consecutive training epochs. The maximum number of epochs is set to be 50.

IV. THE IMPLEMENTATION OF ROBOT CALIBRATION FOR PMC6VA030 ROBOT

A. THE MEASUREMENT SAMPLES

In the robot calibration process, the first step is to generate a large set of different configurations and applied loads. The experiment testbed is a PMC6VA030 industrial robot with 30 kgf payload and 1800 mm reach in this case. Totally 168 measurable poses except singularity were selected out of 225 robot configurations of which each positioning point was 200 mm apart from any neighboring positioning point along any axis inside the robot workspace: X (800, 1600)mm, Y (−800, 800)mm, Z (600, 1400)mm.

B. THE DESIGN OF EXPERIMENT CONSIDERING PAYLOAD EFFECT

It has been shown that different locations of retro-reflector on a link can produce different link deformations [7]. Therefore, it is necessary to design an experiment to consider the payload effect in the robot calibration process. Herein, several experiment-used loading blocks, i.e., 1kg, 2kg, 3kg, 5kg, and 10kg, were designed to attach to the robot end-effector for meeting the experimental plan requirements as shown in Fig. 5.

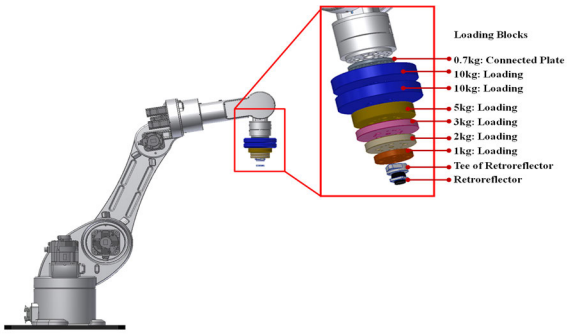

FIGURE 5. The experiment-used loading blocks used for different experiment combination.

C. THE SETUP OF MEASUREMENT SYSTEM

The measurement system consists of two main subsystems, i.e., the robot subsystem and laser tracker subsystem. The PMC6VA030 robot with repeatability of 0.05 mm is calibrated in this case. Its motion command was programmed using an EtherCAT-based robot controller, namely iRUBY, which was also developed by PMC. An apparatus is used to measure the position data of the robot end-effector, which is a FARO VANTAGE^{E} laser tracker. Its measuring accuracy is $(16 + 0.8/\text{m})\ \mu$m within 50 m.

In order to investigate positioning error of the robot, an end-effector, which can be connected to the loading blocks and hold the retroreflector, is designed and setup for obtaining the measured samples as shown in Fig. 6.

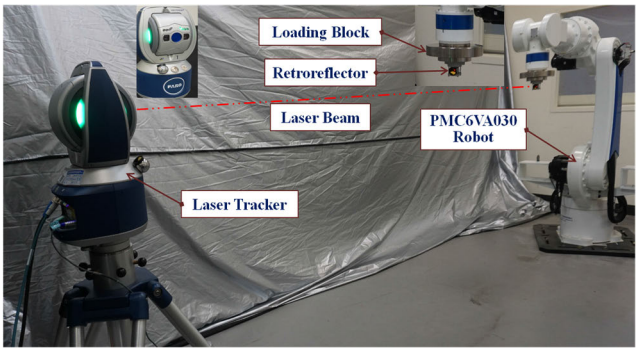

FIGURE 6. Experimental setup integrates the PMC6VA030 robot and Faro laser tracker.

D. THE PREPARATION FOR KINEMATIC CALIBRATION

There are two ways to implement the kinematic calibration:

a) In the case of without considering the effects of loading and configurations, each joint angle of the 168 measurements was obtained via the inverse kinematic computation using the nominal DH parameters, as shown in Fig. 7.

b) In the case of without loading effects but with the consideration of configuration effects, the 168 poses were randomly divided into two parts: 112 configurations were used for calibration while the other 56 configurations were used for cross validation as shown in Fig. 8.

TABLE 3. Hyperparameters of SOMM-ANN model used to predict errors on x-y-z axes.

Layers	X-axis model		Y-axis model		Z-axis model	
	Number of neurons	Activation	Number of neurons	Activation	Number of neurons	Activation
Layer 1	20	Tanh	100	Relu	50	Tanh
Layer 2	20	Tanh	50	Relu	50	Tanh
Layer 3	20	Tanh	-	-	40	Tanh
Layer 4	20	Tanh	-	-	30	Tanh
Layer 5	10	Tanh	-	-	-	-
Layer 6	20	Tanh	-	-	-	-

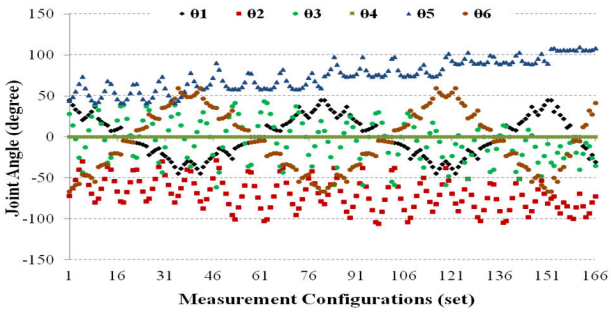

FIGURE 7. The joint angle of 168 configurations used for kinematic calibration.

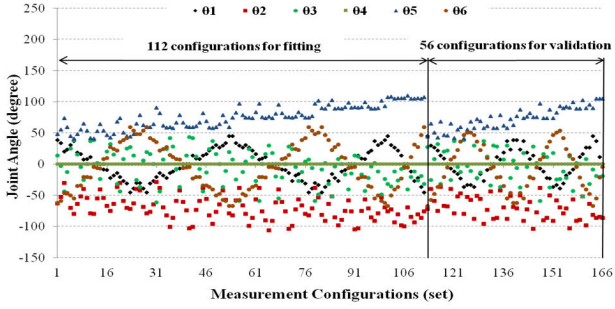

FIGURE 8. The 112 configurations used for fitting and 56 unfitted configurations used for cross validation.

E. THE PREPARATION FOR ANN-BASED CALIBRATION

The training, validating, and testing data have to be prepared for artificial neural network calibration with the consideration of loading and configuration effects. Besides the nominal kinematic model, the parameters in the transformation matrix, $\boldsymbol{A}_{\boldsymbol{0}}^{\boldsymbol{s}}$ and the translation matrix $\boldsymbol{A}_{\boldsymbol{T}}^{\boldsymbol{6}}$ of the robot-laser tracker measurement system should be calibrated together with the kinematic parameters in order to obtain better performance during the parameter identification process. The experimental design is used to establish the configuration-loading datasets for training, validating, and testing the ANN model used in this paper is shown in Fig. 9.

a) Group A: Case with partially untrained loading conditions and without untrained configurations. It is noted that as shown in Fig. 9, for this group the applied loads are divided into two parts, i.e., GA10 and GA20. The GA10 dataset

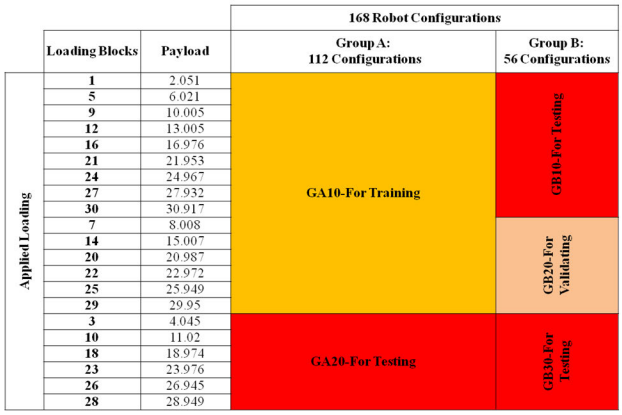

FIGURE 9. The experimental design for configuration-loading datasets used for training, validating, and testing of ANN model.

used for training can totally produce 1680 combinations from the collection of 112 robot configurations and 15 loading conditions; GA20 dataset used to test the trained ANN model can totally produce 672 combinations from the collection of 112 trained robot configurations and 6 untrained loading conditions.

b) Group B: Case with partially untrained loading conditions and untrained configurations: For Group B in Fig. 9, the applied loads are divided into three parts, i.e., GB10, GB20, and GB30. This group mainly tries to further understand the untrained robot configuration effects. The GB20 dataset is used to validate the ANN model, which produces 336 combinations from the collection of 56 untrained configurations and 6 trained loading conditions; GB10 and GB30 are used for testing the trained ANN model, which produces totally 840 combinations from the collection of 56 untrained configurations and 15 loading conditions including 9 trained and 6 untrained.

V. RESULTS AND DISCUSSIONS

A. KINEMATIC CALIBRATION USING BFGS OPTIMIZATION APPROACH

1) WITHOUT LOADING AND CONFIGURATION EFFECTS

Because different applied loading conditions will cause the deviation of positioning error for certain kinematic model, the nominal kinematic parameters should thus be identified

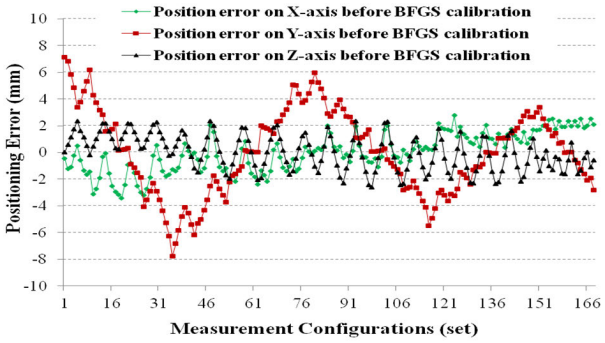

FIGURE 10. The deviation of positioning error on X-Y-Z axis at different configuration before kinematic calibration.

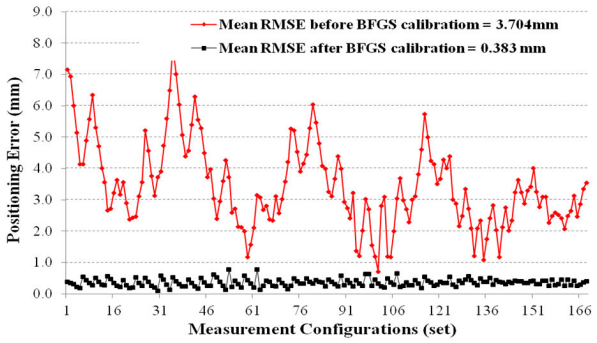

FIGURE 11. The comparison of RMSE between before and after kinematic calibration.

without considering the loading effects in the identification process. We firstly identify 34 parameters, which include 25 geometric parameters listed in TABLE 1, six base coordinates, and three tool position coordinates, from the 168 robot configurations using the aforementioned BFGS optimization algorithm. The solution of the BFGS optimization produces the following results: Root mean square error (RMSE) after base alignment 3.704 mm, standard deviation 1.351 mm, and maximum error 7.909 mm. Hence, the positioning error of the PMC6VA030 robot without payload is about 3.704 mm before calibration.

Fig. 10 shows the deviation of positioning errors in X-Y-Z coordinate system at different measurement configurations before kinematic calibration. In view of Figs. 7 and 10, a significant positive relationship between joint angle $\{\theta_1, \theta_6\}$ and in particular, prominent positioning errors in Y-direction have been observed in Fig. 10. The deviations of the positioning error for different numbers of configuration between before and after kinematic calibrations are shown in Fig. 11. After the kinematic calibration has been done, the mean RMSE is improved to 0.383 mm, standard deviation reduced to 0.161 mm, and maximum error reduced to 0.556 mm. The improvement percentage of the mean RMSE is 89.7% when compared with the condition before calibration. This improvement percentage coincides with that obtained in the previous research [24], which illustrated that approximately 90% of the positioning error of the industrial robot was caused by kinematic parameters. Furthermore, the small difference between the present mean RMSE of 0.383 mm and the RMSE of 0.399 mm obtained using the commercial software "Spatial Analyzer", which is developed by FARO, also validates the accuracy of the proposed BFGS optimization approach. After using the BFGS optimization algorithm for calibration, the updated values of the geometric parameters listed in TABLE 1 is listed in TABLE 4.

The above case used the totally 168 configurations to fit for obtaining optimal parameter set proved the effectiveness. However, it's hard to collect all possible robot configurations for optimization fit within the robot workspace, using specific samples for fit in order to predict unfit ones are the fact in practical applications. To discuss this kind of case is of necessity.

TABLE 4. The identified kinematic parameters of PMC6VA030 robot.

Joint i	a_{i-1}	α_{i-1}	β_{i-1}	d_i	θ_i
1	-3.568	179.876	-	-599.739	-0.009
2	270.017	89.962	-0.006	-0.010	0.157
3	800.882	-0.005	-	-0.010	-0.660
4	140.026	89.948	-	-737.945	-0.037
5	0.026	-89.863	-	-0.010	-0.141
6	0.032	-90.045	-	228.559	0.000

2) CONFIGURATION AND LOADING EFFECTS

The previous results did not consider the applied loading and configuration effects. The experimental design described in the sub-paragraph D of the previous section will be used to study the configuration effects on the BFGS kinematic calibration with. Herein, in the first stage, 112 configurations were used in the BFGS kinematic calibration to determine the optimal geometric parameters. In the second stage, the optimal geometric parameters were used to predict the positioning errors of the rest (56) configurations.

Fig. 12 shows comparative results of RMSEs before and after BFGS kinematic calibration, in which the positioning error after calibration was uniformly reduced to an acceptably small value in the first segment and second segment appeared randomly deviation; The mean RMSEs with configuration effects involved in the second segment would be larger than those without configurations effects in the first segment. It is also observed that the positioning error could be significantly affected by the robot configurations during the calibration process.

It is noted that loading effect was not included in the above kinematic calibration process. To consider loading effect, the identified kinematic parameters listed in TABLE 4 were substituted into robot controller to compute the robot position with applied loadings. The result is shown in Fig. 13. From the figure, it is obvious that the mean RMSE increased as applied loading increased. The mean RMSE increased to 0.94 mm as the payload lied in its maximum value.

3) ERROR RESULTS AND ANALYSIS

In view of the above results, it seems worthy to analyze and discuss the following key issues:

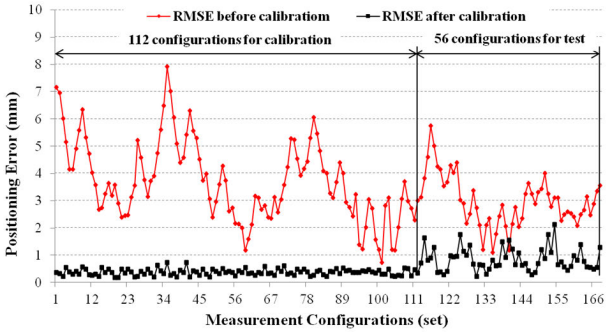

FIGURE 12. The comparison of RMSE between before and after kinematic calibration, as well as cross validation.

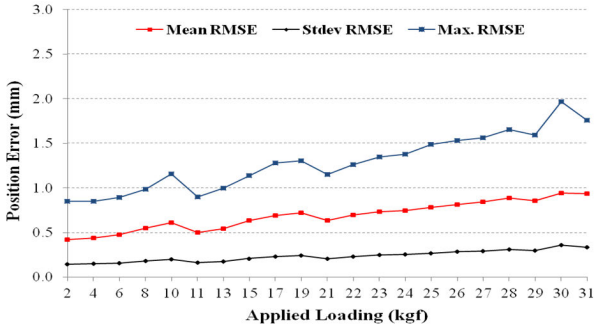

FIGURE 13. The deviations of RMSE under different applied loadings within maximum payload.

(1) The comparisons of the residual position errors in the X, Y, and Z directions before- and after BFGS kinematic calibration using the testing dataset are obtained as shown in Fig. 14. Some brief conclusions can be drawn:

a) Residual positioning error in Y direction is the largest error after BFGS calibration and is also getting larger as the loading is increased; the values are still largely up to 1.5 mm.

b) Residual positioning error on Z axis is the smallest error among X, Y, and Z axes errors after BFGS kinematic calibration. It is no significant effect in this case due to the specific configurations for measurement.

c) Residual positioning error on X axis shows a minor effect of loadings. Some values are still large up to 1 mm.

(2) Fig. 15 is the relationship between residual positioning error on Y-axis with joint angle $\{\theta_1,\theta_6\}$. It is obvious that the residual errors were highly positive correlation with joint angle $\{\theta_1\}$ and negative correlation with joint angle $\{\theta_6\}$. It can be effective to train and compensate the positioning error according to the function of joint angle.

(3) Fig. 16 is the bi-variate kernel distribution, histogram and scatter plot of X, Y, and Z axes' residual positioning errors after BFGS kinematic calibration, in which existed two significant phenomenon:

a) The residual positioning errors of X, Y, and Z axes were highly uncorrelated for one another, the result using traditional MOSM-ANN to model the three-axis error was not satisfied.

b) A bi-model distribution existed on X-axis error, and this will be difficult to model it.

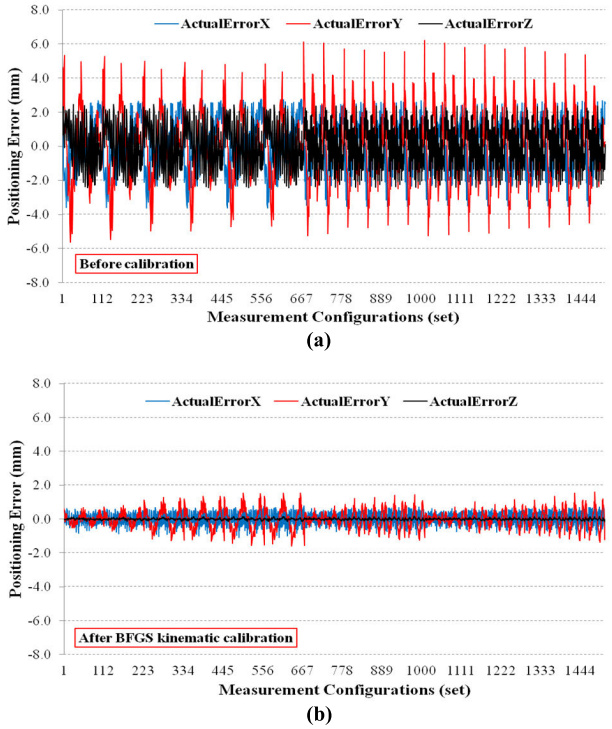

FIGURE 14. The positioning errors on X, Y, and Z axes (a)before- (b)after-BFGS kinematic calibration using testing data.

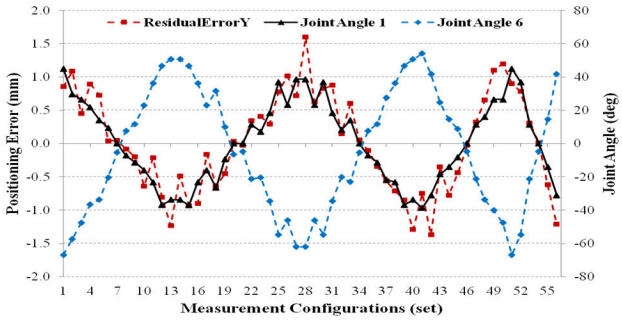

FIGURE 15. The relationship between residual positioning error on Y-axis with joint angles after BFGS kinematic calibration.

4) AN INTERIM SUMMARY

The above results can lead to the following points:

(1) The kinematic calibration using the BFGS algorithm can significantly reduce the mean RMSE error to 0.403 mm with the consideration of configuration effects.

(2) The mean RMSEs increased as the applied loading increased, which will up to 0.94 mm as the payload lied in the maximum value.

(3) After kinematic calibration, the use of the identified parameters to predict the position of the industrial robot without considering configuration effects but considering loading effects still produces relatively large position error.

(4) When payload effect is not included in the kinematic calibration, the positioning accuracy is not enough for the precision positioning applications. A further step for improving the non-geometric errors involving configuration and payload effects becomes essential.

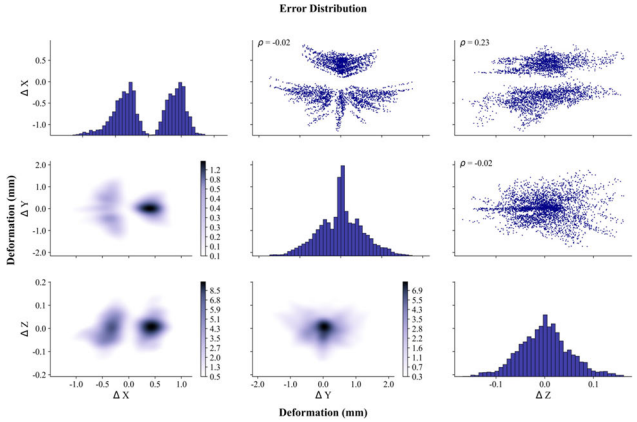

FIGURE 16. The bi-variate kernel distribution, histogram and scatter plot of X, Y and Z axes errors.

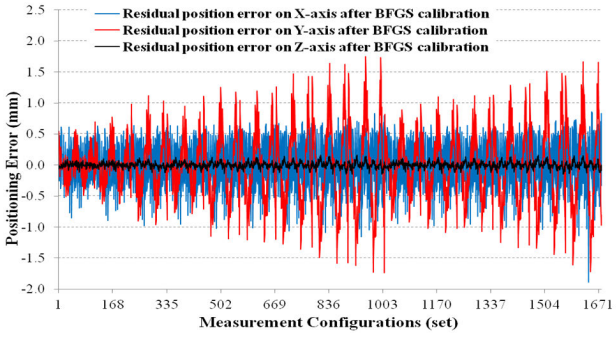

FIGURE 17. The positioning errors on X-Y-Z axes after BFGS kinematic calibration used as SOMM-ANN output data.

B. NON-KINEMATIC CALIBRATION USING SOMM-ANN APPROACH

1) FOR SOLVING THE UNCORRELATED ON X, Y, AND Z AXES' ERROR USING SOMM-ANN

After the kinematic calibration, the residual positioning errors were still not low enough to satisfy the requirements of precise tasks, especially when the loading and configuration effects were presented. For overcoming the residual positioning errors of X, Y, and Z axes after BFGS calibration with highly uncorrelated for one another, the SOMM-ANN approach was, therefore, employed to further reduce the residual positioning errors with nonlinear properties with the consideration of different conditions of loading and configuration.

According to the residual positioning error analysis, the proposed SOMM-ANN was implemented firstly. For training the SOMM-ANN model, in view of Fig. 9, the applied loadings and robot joint angles based on robot configurations in the GA10 dataset were used as the input data; the residual positioning errors of GA10 dataset after BFGS kinematic calibration were displayed in Fig. 17 and were used as output data of SOMM-ANN model. The input data and output data were then used to train the SOMM-ANN model in order to further reduce the non-geometric errors after BFGS calibration.

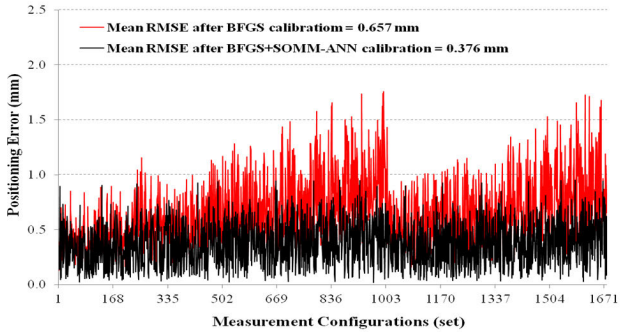

FIGURE 18. The residual positioning error of PMC6VA030 robot used for training model (before and after SOMM-ANN calibration).

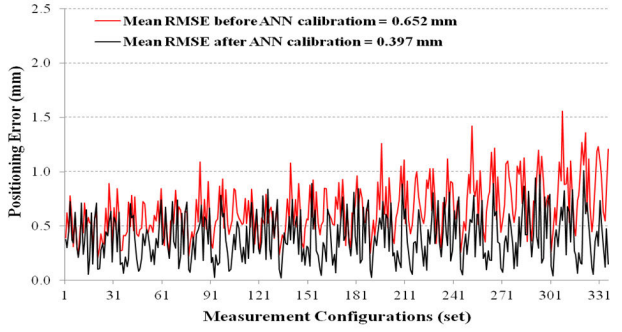

FIGURE 19. The residual positioning error of PMC6VA030 robot used for validating the trained model (before and after SOMM-ANN calibration).

As a result, the mean RMSE of the trained SOMM-ANN model was reduced from 0.657 mm after BFGS calibration to 0.376 mm, up to 42.8% improvement, as shown in Fig. 18. The trained SOMM-ANN model was then used to perform the validation using GB20 dataset with untrained loadings and configurations. The mean RMSE was also reduced from 0.652 mm to 0.397 mm, is shown in Fig. 19. Comparing with training result, they are very close and give an evidence to prove the effectiveness of the train SOMM-ANN model. For testing the trained ANN model, GA20, GB10, and GB30 datasets were used based on different loading and configuration. The result is shown in Fig. 20. It is observed that the residual positioning errors could remain consistent in different datasets, whether the applied loading and robot configurations were trained or not. The test result after compensation of the trained SOMM-ANN showed that the mean RMSE not only can be improved to 0.381 mm but also can overcome the loading and robot configuration effect, even if the untrained loading and configuration were applied on it. The values of mean, standard deviation, and maximum of residual positioning errors on PMC6VA030 industrial robot after SOMM-ANN compensation are also shown in TABLE 5.

2) ERROR ANALYSIS

Comparing the residual positioning errors of before- and after SOMM-ANN calibration from Fig. 21(a) and Fig. 21(b), the results show that SOMM-ANN can effectively improve

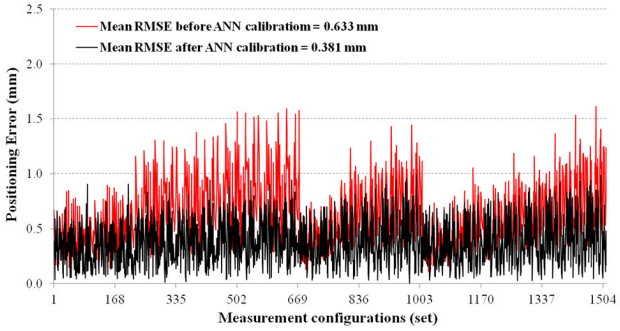

FIGURE 20. The residual positioning error of PMC6VA030 robot used for testing the trained model (before and after SOMM-ANN calibration).

TABLE 5. The errors of PMC6VA030 robot after SOMM-ANN calibration.

Status	Mean	Standard Deviation	Maximum
For Training (mm)	0.376	0.204	0.954
For Validating (mm)	0.397	0.223	1.010
For Testing (mm)	0.381	0.213	0.991

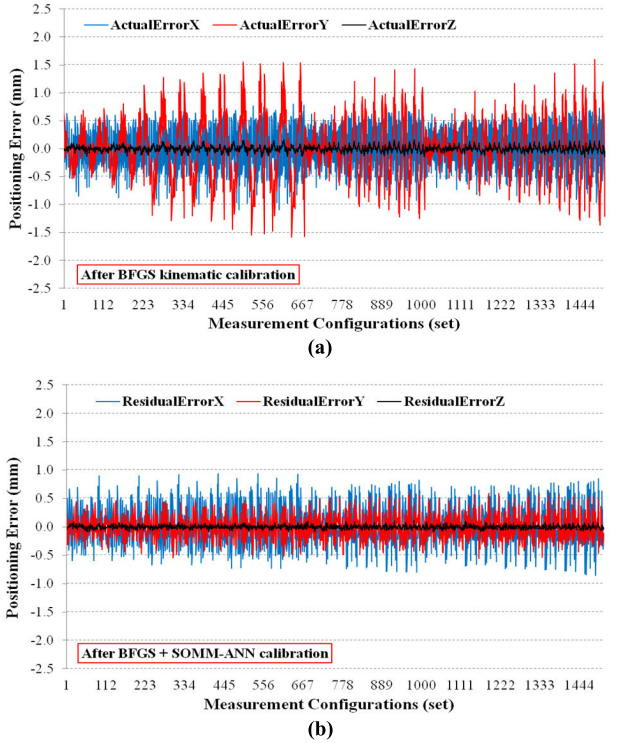

FIGURE 21. The positioning errors on X, Y, and Z axes (a)before- (b)after-SOMM-ANN using testing data.

the effects of loading and configuration, and the residual positioning error was reduced to an acceptably small value on Y and Z axes; but there was no obvious improvement on the X direction due to affected by the bi-model distribution, of which causal is described as below.

The causal for the bi-model distribution case can be explained using the errors which were induced by the deformation of the 2nd link and the twist of the 3rd joint caused from the consequent link weight and applied moment. When the joint angle A_1 at 0 degree, the produced error is located at -Y direction; as the joint angle A_1 moves to -180 degrees, the produced error will be located at -X direction; However, when joint angle A_1 moves to 180 degree, the produced error will be located at X direction; even if the angles of A_2-A_6 are the same, the produced errors are completely opposite. This is the reason why the X-axis error has bi-model distribution, detailed as shown in Fig. 22.

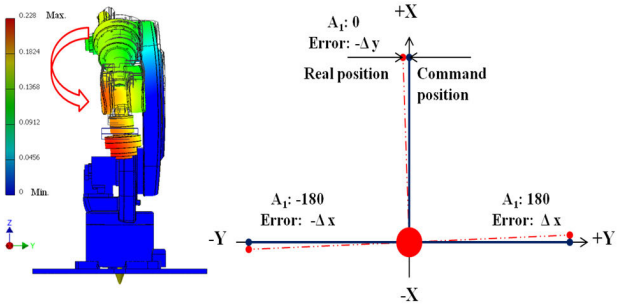

FIGURE 22. The causal of bi-model distribution.

3) FOR SOLVING THE BI-MODEL CASE USING CLASSIFIED-ADDED SOMM-ANN

In order to improve the performance of the previously proposed SOMM-ANN model, a distribution analysis of the error in the direction of each axis was performed. It is evident that the positioning errors in the directions of X, Y and Z axes were highly uncorrelated. Moreover, the error for each axis was modeled with respect to robot configurations and applied loading. Residual positioning errors on X-axis could not be reduced to a reasonable value due to its output data had bi-model distributions. This case would enlarge the error when the prediction was located on the opposite side than actual. Therefore, a classified-added SOMM-ANN (called CA-SOMM-ANN) was investigated to solve the problem in this article. The new concept is to divide the training data into two classes, and then used them to train for obtaining the classifier and two SOMM-ANN models (Model-A, Model-B), respectively. The selected model is determined according to the classified result of input data using trained classifier for validating and testing datasets. The structure of CA-SOMM-ANN is shown in Fig. 23. In this study, a histogram-based gradient boosted decision tree [23] was applied as classification model. The maximum depth of trees, maximum leaf nodes and minimum sample leaves of decision tree is determined by hyperparameter optimization approach using 'Tree of Parzen Estimators' [21] approach provided in the Hyperopt/Python library [22]. The hyperparameters are listed at the end of paragraph 1 of Section V B3. Hyperparameters of this classifier were as follows; (a) Maximum depth of trees = 3, (b) maximum leaf nodes = 60, (c) Minimum sample leaves = 66, (d) learning rate = 0.001 and (e) maximum number of iterations = 300. Binary cross-entropy loss as shown in (27)

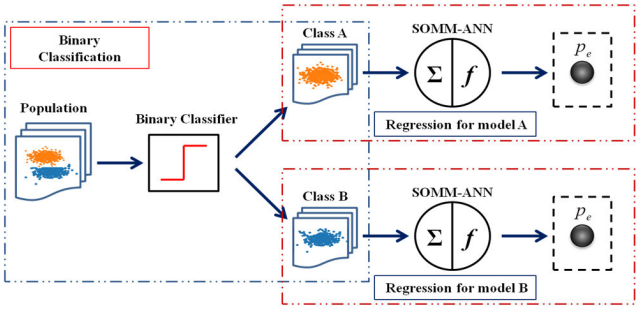

FIGURE 23. The concept and structure of CA-SOMM-ANN.

was applied for training the classifier.

$$loss = -\hat{\mathbf{y}} \log(\mathbf{y}) + \left(1 - \hat{\mathbf{y}}\right) log(1 - \hat{\mathbf{y}}) \tag{27}$$

where $\mathbf{y}$ is the actual class and $\hat{\mathbf{y}}$ is the predicted class by the classifier.

For solving the bi-model distribution case, the CA-SOMM-ANN was used. The input data were the same with SOMM-ANN used for training data, and the output data were the residual positioning error after BFGS calibration. These data were divided into two classes according to the error distribution to train the classifier and error models. The GA20, GB10, and GB30 datasets were used to test the trained CA-SOMM-ANN model. Fig. 24 shows that the mean RMSE was further reduced to 0.296 mm for testing after the CA-SOMM-ANN calibration.

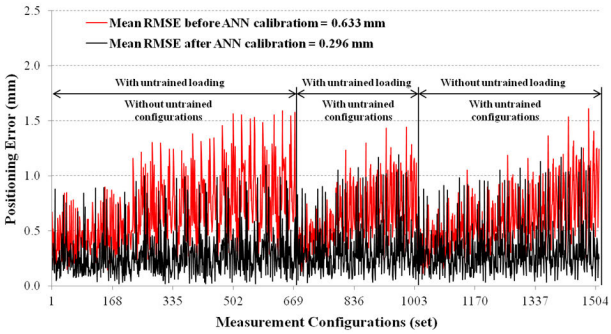

FIGURE 24. The residual positioning error of PMC6VA030 robot for testing (before and after CA-SOMM-ANN calibration).

The mean RMSE was further reduced to 0.296 mm for testing after the CA-SOMM-ANN calibration. From Fig. 25 shows the comparison of residual positioning error on X direction before and after the CA-SOMM-ANN calibration. From the width reduction of red line could obviously appear the effectiveness of the CA-SOMM-ANN calibration approach for solving the bi-model distribution problem.

4) AN INTERIM SUMMARY

From above results and discussions, it could be summarized into several points:

(1) The results show that SOMM-ANN can effectively improve the loading and configuration effects.

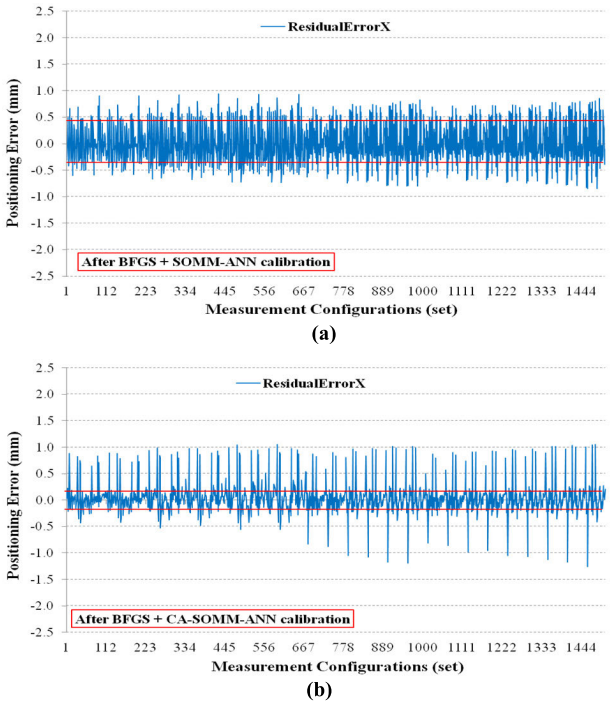

FIGURE 25. RMSEs in X-direction (a) before- (b) after- CA-SOMM-ANN.

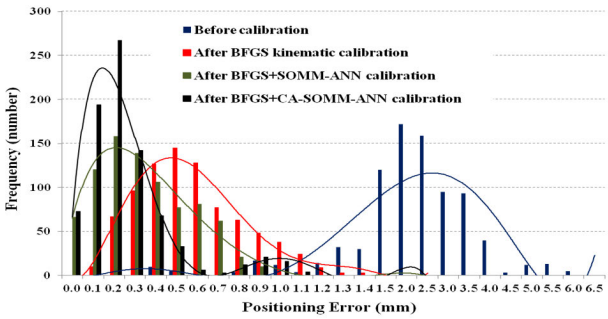

FIGURE 26. The comparison of calibration results using different approaches.

(2) The use of CA-SOMM-ANN for solving the bi-model distribution problem on X-axis error is validated using dataset G230. The result shows that the mean RMSE was reduced from 0.381 mm by SOMM-ANN to 0.296 mm by CA-SOMM-ANN under 93% classification rate.

C. THE COMPARISON OF CALIBRATION RESULTS

Here, the after calibration results obtained from BFGS kinematic calibration and ANN-based calibration, involve SOMM-ANN, and CA-SOMM-ANN with untrained loadings and configurations consideration, are compared with the errors before calibration and with each others. The results are expressed by histogram and probability distribution to represent their distribution, shown in Fig. 26. The mean, standard deviation, and maximum of positioning error after calibrations are shown on TABLE 6. From these results, the performance of each calibration approach is displayed and

compared. This also can be used to validate the effectiveness of the proposed method in this paper.

TABLE 6. The positioning errors of PMC6VA030 robot after calibrations.

Before/After Calibration	Mean	Standard Deviation	Maximum
Before calibration	2.613	1.015	6.294
After BFGS kinematic	0.618	0.275	1.609
After BFGS+SOMM-ANN	0.389	0.991	0.991
After BFGS+CA-SOMM-ANN	0.310	0.213	1.255

VI. CONCLUSION

In this work, a hybrid robot calibration approach was presented to compensate both kinematic and non-kinematic errors on PMC6VA030 industrial robot for attaining high positioning accuracy of the robot. The robot was calibrated not only with a focus on the geometric error and non-geometric errors, but also considering the robot configuration and applied loading effects for realistic engineering applications. The first step is to adopt the BFGS technique used to alternate the Hessian and Jacobian matrix of second derivatives in the kinematic calibration process for obtaining better robustness and efficiency. The second step is to propose an ANN-based calibration, include SOMM-ANN, and CA-SOMM-ANN for further reducing the residual positioning error of the robot. The final results obtained by the CA-SOMM-ANN show the mean/maximum residual positioning errors are reduced from 2.613mm/6.294mm to 0.310mm/1.255mm on 840 untrained measurement data, respectively; up to 88.1% and 80.1% improvement than before calibration. The advantages indicate the effectiveness and confirm the robustness of the proposed method. Some conclusions can be drawn as follows:

(1) The proposed BFGS kinematic calibration is useful to improve the positioning error on geometric error. But the identified parameters used to predict the position of an industrial robot with unfitted configurations and with fitted loadings were still existing larger positioning error. The mean RMSEs were increased as applied loadings were increased within the maximum payload.

(2) Applied loadings and robot configurations significantly affect the positioning accuracy of an industrial robot; just kinematic calibration was not enough for those precise tasks. A next step for further improving the residual positioning errors with configuration and loading effects is inevitable.

(3) It is observed that the position of robot end-effector has a higher effect on the axis error than the payload applied on it.

(4) The used ANN-based in this paper, includes SOMM-ANN and CA-SOMM-ANN, can both effectively compensate the errors caused by loading and robot configuration effects simultaneously.

(5) Only CA-SOMM-ANN approach is suitable to solve for those models with bi-model distribution nature.

For future research directions, it is worthwhile to seek further applications of the hybrid calibration approach to real engineering, as well as other types of industrial robots. In this study, we just considered positioning error only, did not consider the effect of orientation error yet. We also did not discuss the algorithm of compensating the model into robot controller. Anyone who is interested in this area can extend our study to the abovementioned topics based on our results. In addition, a path experiment study to test and validate the performance of the algorithm is also recommended.

REFERENCES

[1] Z. Roth, B. Mooring, and B. Ravani, "An overview of robot calibration," *IEEE J. Robot. Autom.*, vol. RA-3, no. 5, pp. 377–385, Oct. 1987.
[2] J. M. Renders, E. Rossignol, M. Bequet, and R. Hanus, "Kinematic calibration and geometrical parameter identification for robots," *IEEE Trans. Robot. Autom.*, vol. 7, no. 6, pp. 721–731, Dec. 1991.
[3] I.-C. Ha, "Kinematic parameter calibration method for industrial robot manipulator using the relative position," *J. Mech. Sci. Technol.*, vol. 22, no. 6, pp. 1084–1090, Jun. 2008.
[4] J. Santolaria and M. Ginés, "Uncertainty estimation in robot kinematic calibration," *Robot. Comput.-Integr. Manuf.*, vol. 29, no. 2, pp. 370–384, Apr. 2013.
[5] C. Mao, S. Li, Z. Chen, H. Zu, Z. Wang, and Y. Wang, "A novel algorithm for robust calibration of kinematic manipulators and its experimental validation," *IEEE Access*, vol. 7, pp. 90487–90496, 2019.
[6] J. H. Jang, S. H. Kim, and Y. K. Kwak, "Calibration of geometric and non-geometric errors of an industrial robot," *Robotica*, vol. 19, no. 3, pp. 311–321, May 2001.
[7] A. Nubiola and I. A. Bonev, "Absolute calibration of an ABB IRB 1600 robot using a laser tracker," *Robot. Comput.-Integr. Manuf.*, vol. 29, no. 1, pp. 236–245, Feb. 2013.
[8] A. Joubair, A. Nubiola, and I. Bonev, "Calibration efficiency analysis based on five observability indices and two calibration models for a six-axis industrial robot," *SAE Int. J. Aerosp.*, vol. 6, no. 1, pp. 161–168, Sep. 2013.
[9] J. Zhou, H.-N. Nguyen, and H.-J. Kang, "Simultaneous identification of joint compliance and kinematic parameters of industrial robots," *Int. J. Precis. Eng. Manuf.*, vol. 15, no. 11, pp. 2257–2264, Nov. 2014.
[10] Y. Guo, S. Yin, Y. Ren, J. Zhu, S. Yang, and S. Ye, "A multilevel calibration technique for an industrial robot with parallelogram mechanism," *Precis. Eng.*, vol. 40, pp. 261–272, Apr. 2015.
[11] K. Kamali, A. Joubair, I. A. Bonev, and P. Bigras, "Elasto-geometrical calibration of an industrial robot under multidirectional external loads using a laser tracker," in *Proc. IEEE Int. Conf. Robot. Autom. (ICRA)*, May 2016, pp. 4320–4327.
[12] M. A. Meggiolaro, S. Dubowsky, and C. Mavroidis, "Identification and compensation of geometric and elastic errors in large manipulators: Application to a high accuracy medical robot," in *Proc. DETC ASME Design Eng. Tech. Conf.*, Sep. 1998, pp. 1–7.
[13] H. N. Nguyen, P. N. Le, and H. J. Kang, "A new calibration method for enhancing robot position accuracy by combining a robot model-based identification approach and an artificial neural network-based error compensation technique," *Adv. Mech. Eng.*, vol. 11, no. 1, Jan. 2019, Art. no. 168781401882293.
[14] G. Gao, H. Zhang, H. San, X. Wu, and W. Wang, "Modeling and error compensation of robotic articulated arm coordinate measuring machines using BP neural network," *Complexity*, vol. 2017, pp. 1–8, Oct. 2017.
[15] M. P. Kumar and S. D. Ashok, "Artificial neural network based geometric error correction model for enhancing positioning accuracy of a robotic sewing manipulator," *Procedia Comput. Sci.*, vol. 133, pp. 1048–1055, Jan. 2018.
[16] D. Wang, Y. Bai, and J. Zhao, "Robot manipulator calibration using neural network and a camera-based measurement system," *Trans. Inst. Meas. Control*, vol. 34, no. 1, pp. 105–121, Feb. 2012.
[17] N. Takanashi, "6 DOF manipulators absolute positioning accuracy improvement using a neural-network," in *Proc. IEEE Int. Workshop Intell. Robots Syst., Towards New Frontier Appl.*, Ibaraki, Japan, Jul. 1990, pp. 635–640.

[18] W. Khalil and J. Kleinfinger, "A new geometric notation for open and closed-loop robots," in *Proc. IEEE Int. Conf. Robot. Autom.*, vol. 3, Apr. 1986, pp. 1174–1179.
[19] S. Hayati and M. Mirmirani, "Improving the absolute positioning accuracy of robot manipulators," *J. Robotic Syst.*, vol. 2, no. 4, pp. 397–413, 1985.
[20] J. S. Arora, *Introduction to Optimum Design*. Amsterdam, The Netherlands: Elsevier, 2004.
[21] J. Bergstra, R. Bardenet, Y. Bengio, and B. Kégl, "Algorithms for hyper-parameter optimization," in *Proc. 24th Int. Conf. Neural Inf. Process. Syst. (NIPS)*, Red Hook, NY, USA, 2011, pp. 2546–2554.
[22] J. Bergstra, D. Yamins, and D. D. Cox, "Making a science of model search: Hyperparameter optimization in hundreds of dimensions for vision architectures," in *Proc. 30th Int. Conf. Mach. Learn. (ICML)*, vol. 28, 2013, pp. 115–123.
[23] A. Guryanov, "Histogram-based algorithm for building gradient boosting ensembles of piecewise linear decision trees," in *Analysis of Images, Social Networks and Texts*. Cham, Switzerland: Springer, 2019, pp. 39–50.
[24] R. Bernhardt and S. L. Albright, *Robot Calibration*. London, U.K.: Chapman & Hall, 1993.

JEN-CHUNG HSIAO received the Ph.D. degree in mechanical engineering from National Chiao Tung University, Taiwan, in 2020. From 2012 to 2020, he was a Division Director of the Robotics & Automation Division. Since 2020, he has been a Chief Technology Director in general manager office, Precision Machinery Research & Development Center, Taichung City, Taiwan. His research interests include mechanical design optimization, reliability engineering, and robot calibration.

KUMAR SHIVAM received the B.S. and M.S. degrees in mechanical engineering and the Ph.D. degree in mechanical and energy engineering from Kun Shan University, Tainan City, Taiwan, in 2017 and 2020, respectively.

From 2015 to 2018, he was a Research Assistant with the Intelligent Vehicle Research Center, Kun Shan University. He has been a Research Engineer with the Robotics & Automation Division, Precision Machinery Research & Development Center, Taichung City, Taiwan, since 2018. His research interests include the machine learning techniques, time series forecasting methods, advance CNN architectures for time series data, optimization algorithms, application of meta-heuristic algorithms, and hybrid energy systems.

I-FANG LU was born in Tainan City, Taiwan, in 1991. She received the M.S. degree in electrical engineering from the National Yunlin University of Science and Technology, Yunlin, Taiwan, in 2016. From 2016 to 2020, she was a Research and Development Engineer with PMC, Taichung City, Taiwan. Her research interests include the development of auto control and Kalman neural networks, and robot control systems.

TAI-YAN KAM received the Ph.D. degree from Northwestern University, USA, in 1981. Formerly the Dean, College of Engineering, he is currently a Professor with the Department of Mechanical Engineering, National Chiao Tung University, Taiwan, Republic of China. His research interests include composite materials and structures, nondestructive evaluation and health monitoring of structural and mechanical systems, robotic automation, acoustics, and wind power.